Electronic Supplementary Information

Deformable Complementary Moisture and Tribo Energy Harvester

Gwanho Kim,[a] Jae Won Lee, [b] Kaiying Zhao,[a] Taebin Kim,[a] Woojoong Kim,[a] Jin Woo Oh,[a] Kyuho Lee,[a] Jihye Jang,[a] Guangtao Zan,[a] Jong Woong Park,[a] Seokyeong Lee,[a] Yeonji Kim,[a] Wei Jiang,[a] Shengyou Li [a] and Cheolmin Park *[a]
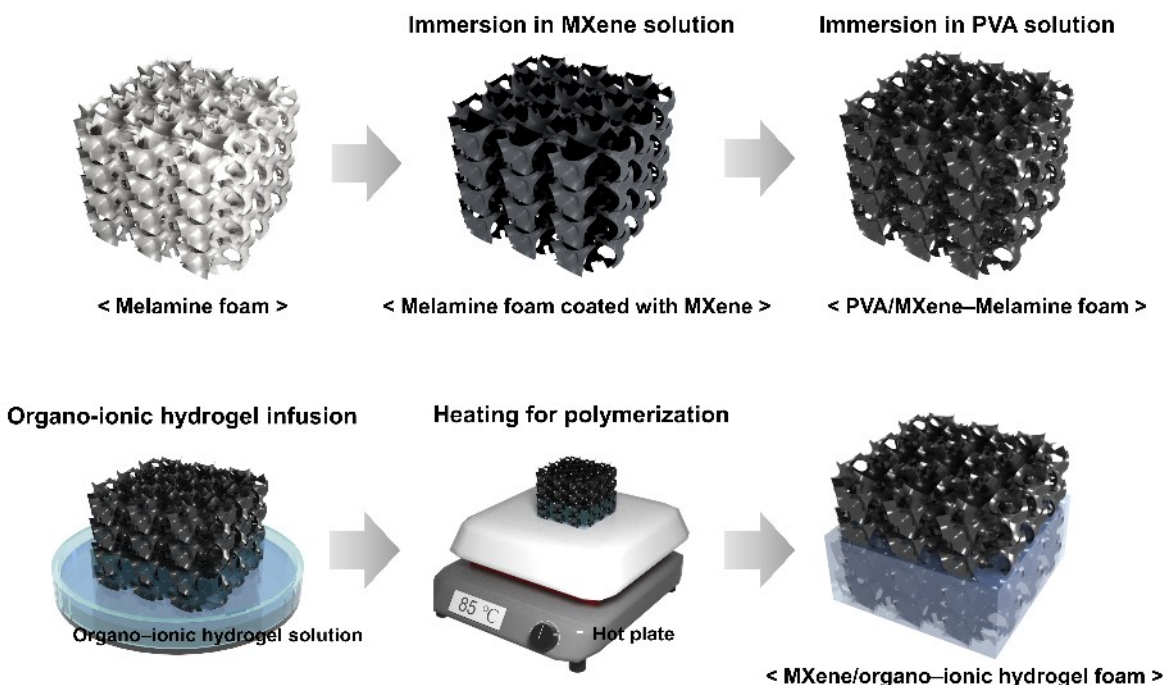
Fig. S1 Schematic of the preparation process of the MXene/organo–ionic hydrogel foam (MOHF) using the dip-coating method and subsequent gelation of the organo–ionic hydrogel.
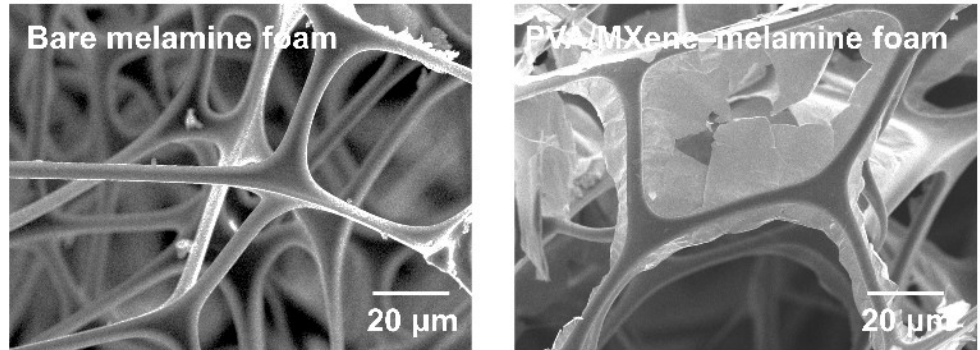
Fig. S2 Low-magnification scanning electron microscope (SEM) images for comparing bare melamine foam and PVA/MXene–melamine foam.
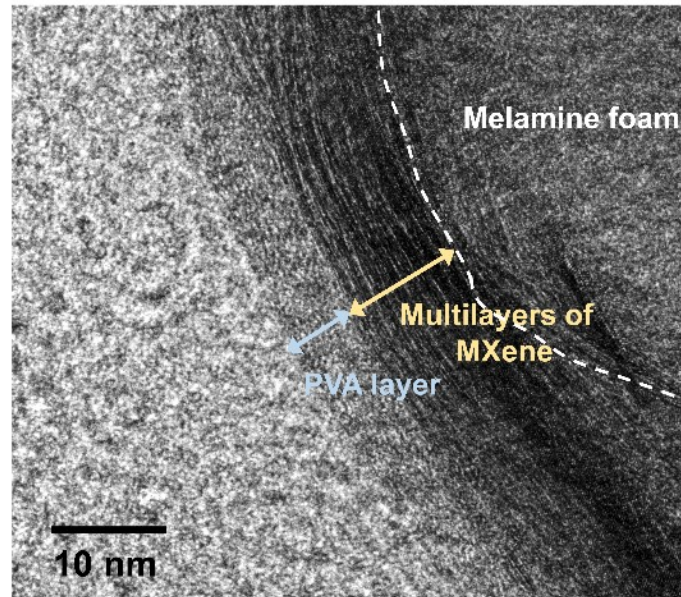
Fig. S3 Cross-sectional high-resolution transmission electron microscope (TEM) image of a single PVA/MXene–melamine skeleton.
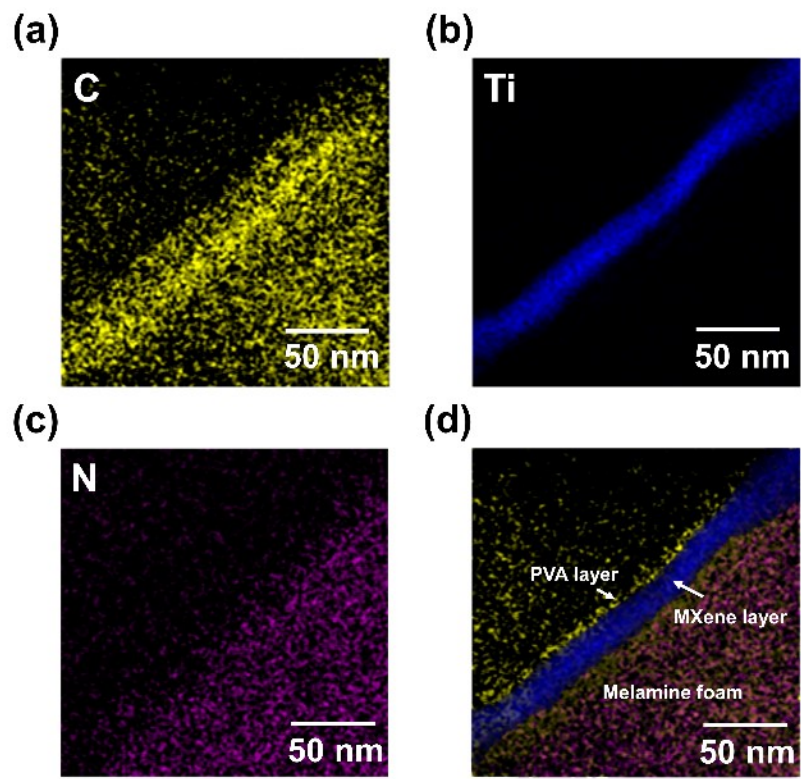
Fig. S4 Energy-dispersive X-ray spectroscopy (EDS) images of a cross-sectional PVA/MXene–melamine skeleton showing (a) carbon, (b) titanium, (c) nitrogen, and (d) merged elements.
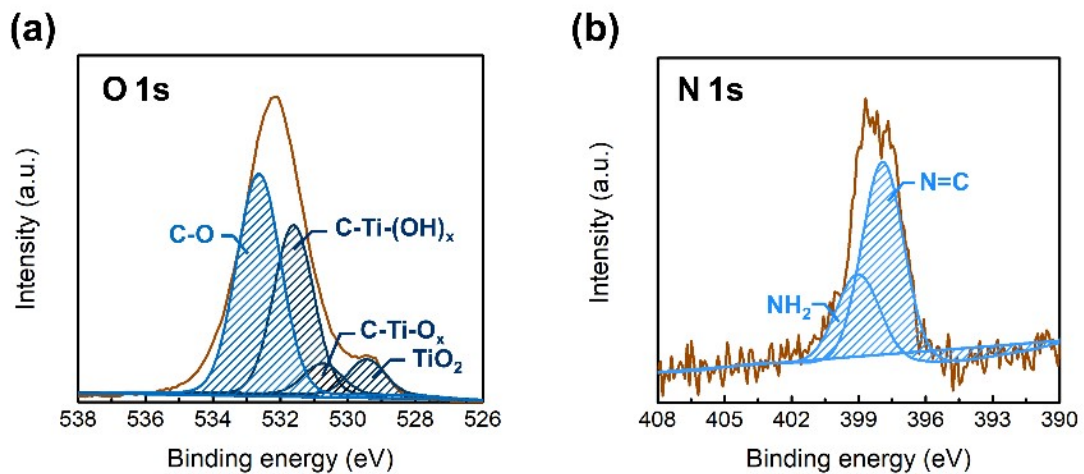
Fig. S5 X-ray photoelectron spectroscopy (XPS) spectra of the PVA/MXene–melamine foam showing (a) O 1s and (b) N 1s peaks.
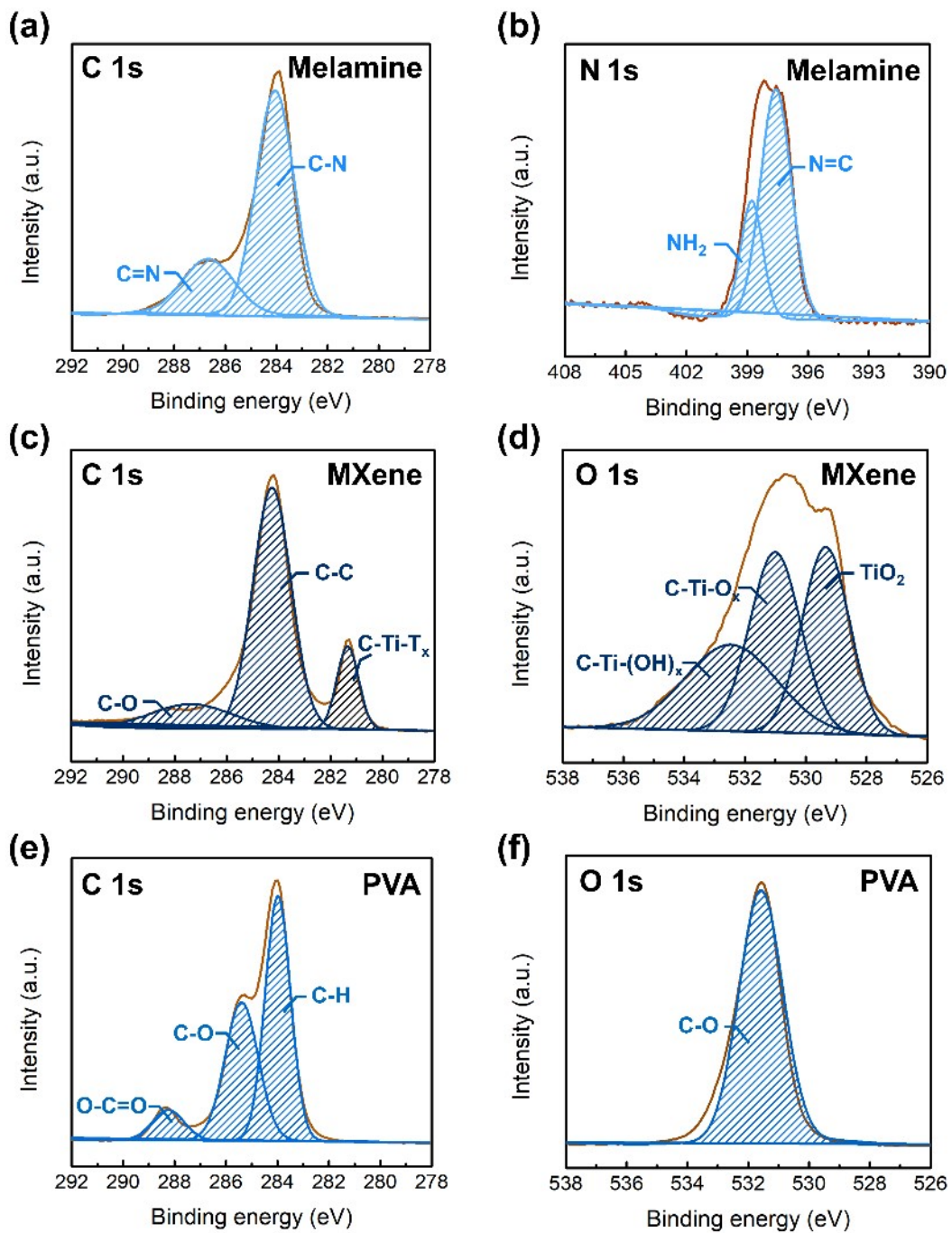
Fig. S6 X-ray photoelectron spectroscopy (XPS) spectra of C 1s, O 1s, or N 1s for (a),(b) melamine foam, (c),(d) MXene film, and (e),(f) poly(vinyl alcohol) (PVA) film.
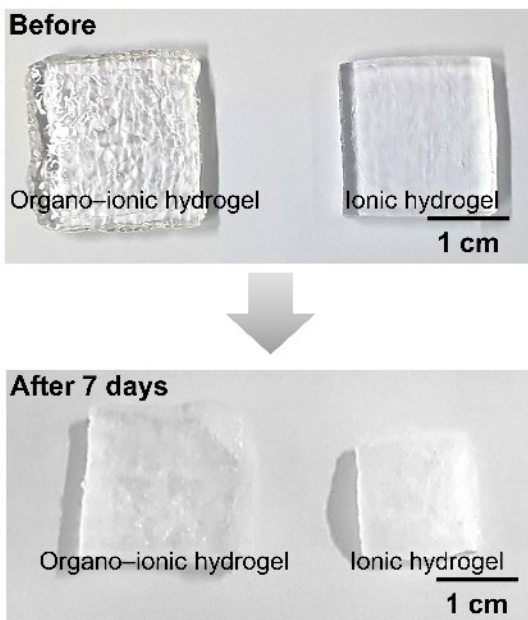
Fig. S7 (a) Photographs for comparing the organo–ionic hydrogel and ionic hydrogel taken at 0 and 7 days under 20% RH. (b) Evaluation of flexibility after 7 days.
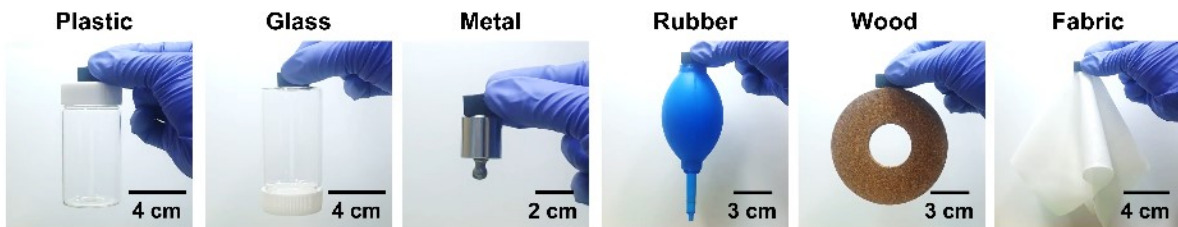
Fig. S8 Adhesion performance of MOHF for various substrates.
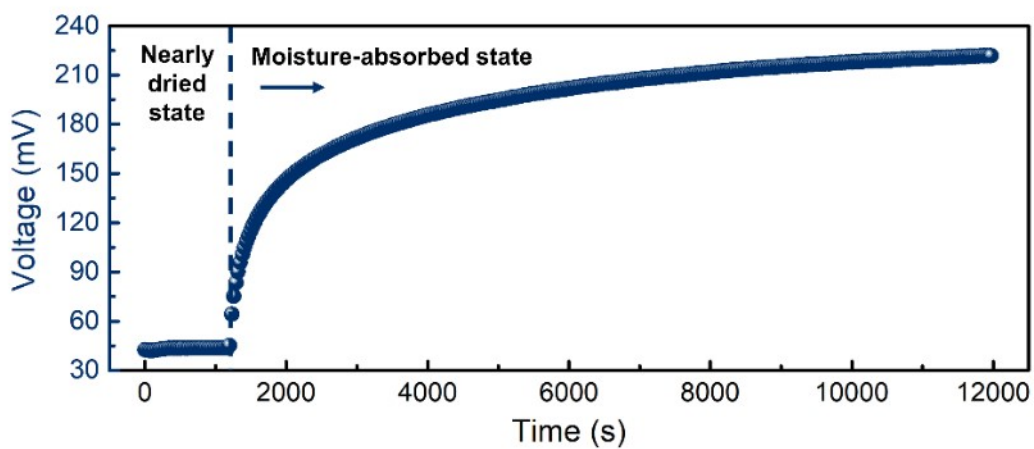
Fig. S9 Open-circuit voltage (V_{OC}) of MEG–MOHF before and after moisture absorption.
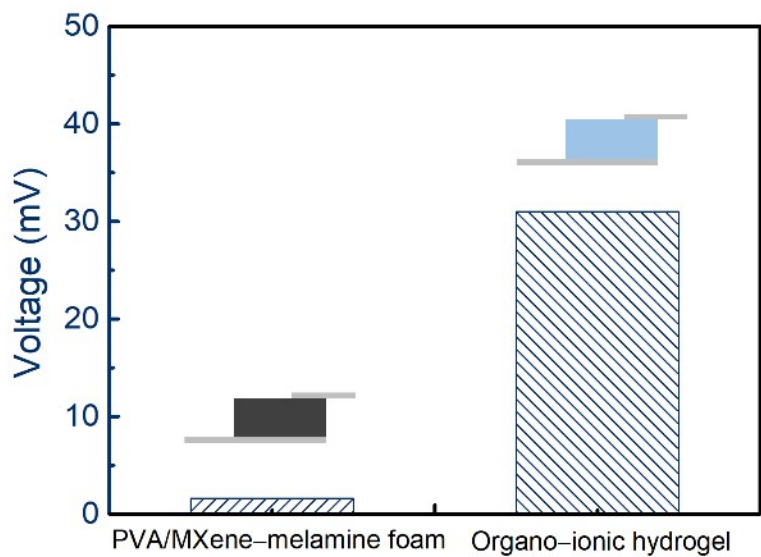
Fig. S10 Open-circuit voltage (V_{OC}) of MEG device with PVA/MXene–melamine foam or organo–ionic hydrogel.
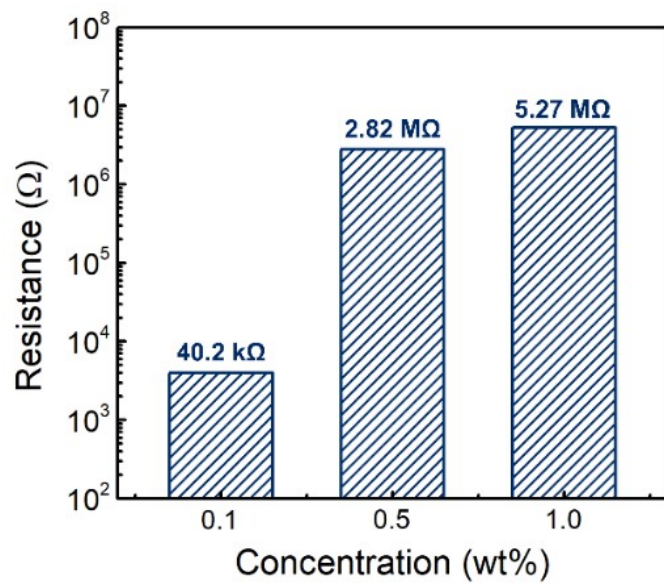
Fig. S11 Resistance of MEG–MOHF device for various concentrations of PVA.
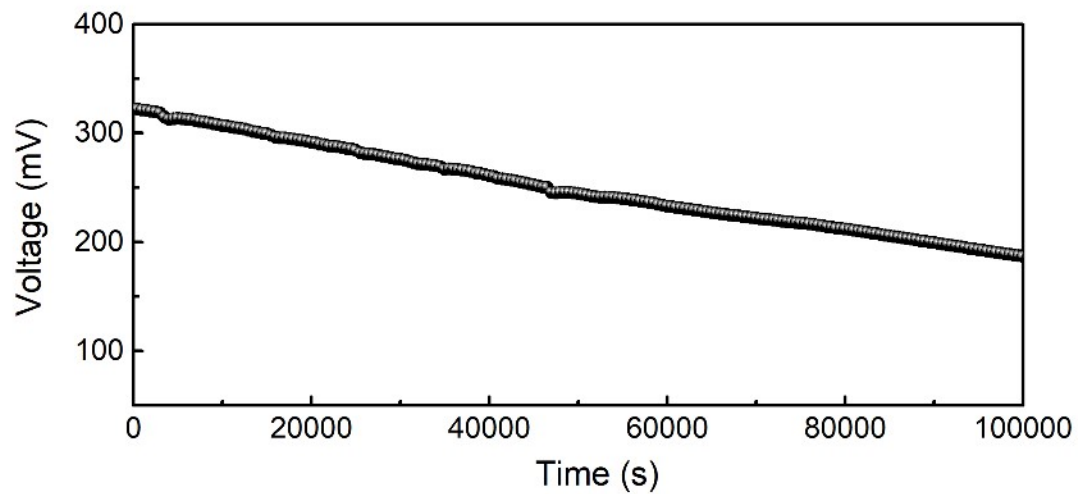
Fig. S12 Continuous measurement of open-circuit voltage (V_{OC}) for the MEG–MOHF device without PVA coating over time under open ambient environment.
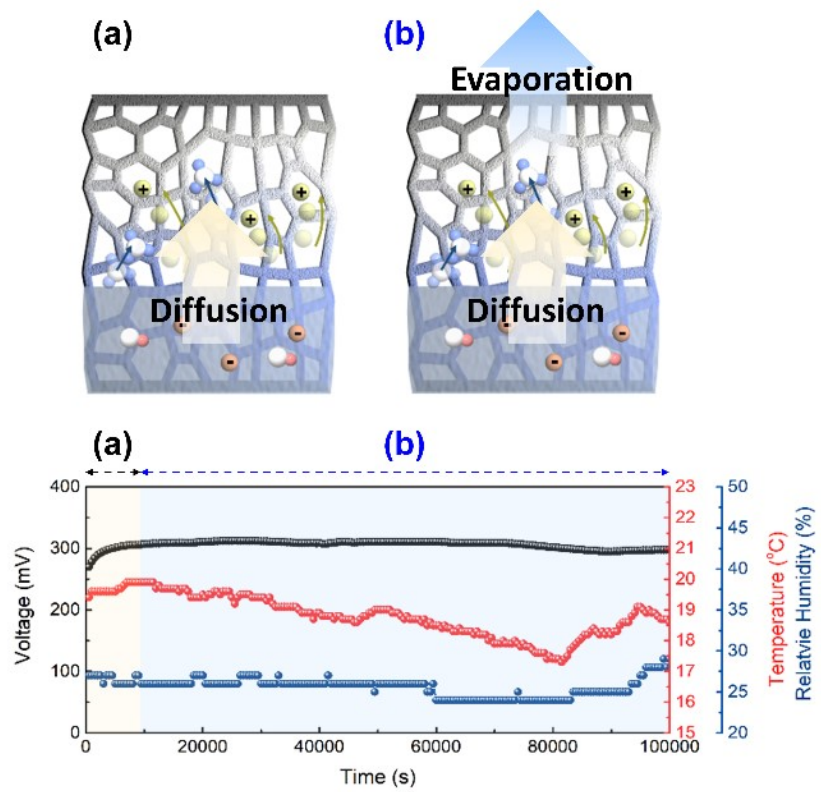
Fig. S13 Schematics and device performance of a MEG–MOHF before (a) and after (b) moisture absorption.
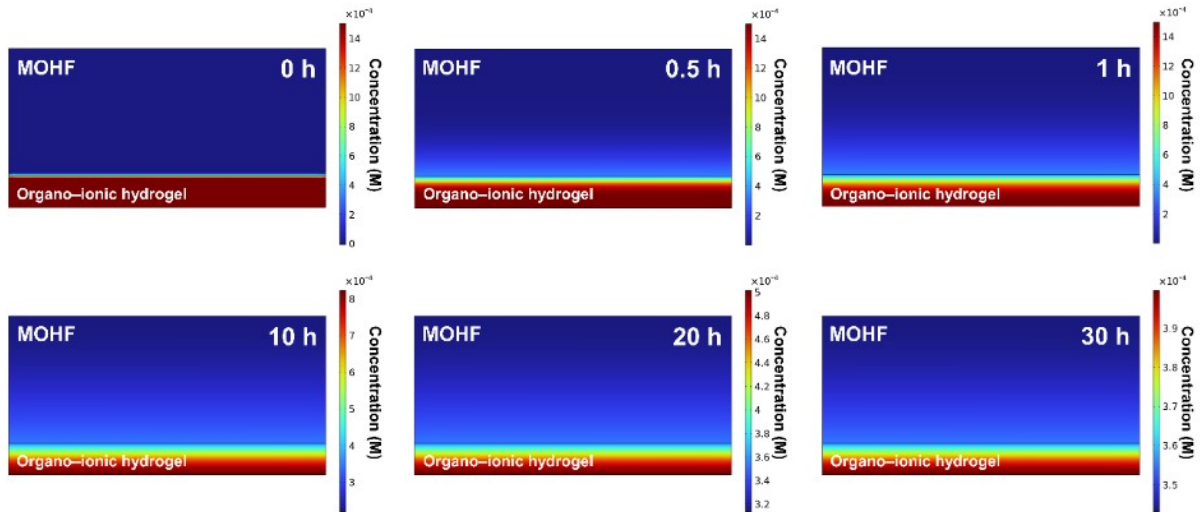
Fig. S14 COMSOL simulation results of the concentration distribution of K^+ over time in the MOHF.
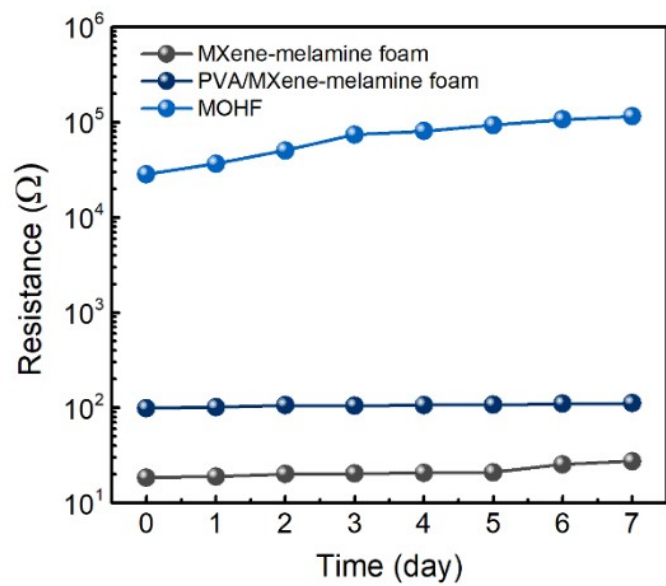
Fig. S15 Resistance change over time for MXene–melamine foam, PVA/MXene–melamine foam, and MOHF.
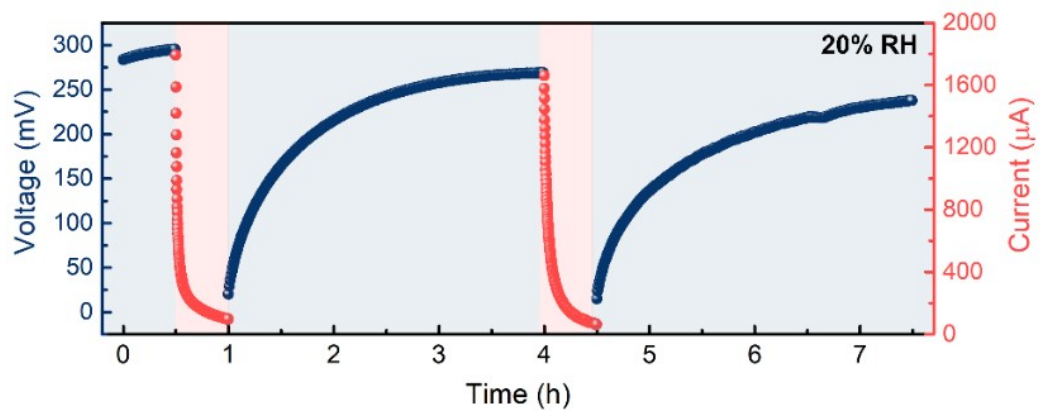
Fig. S16 The discharging and charging properties of the MEG–MOHF at 20% RH.
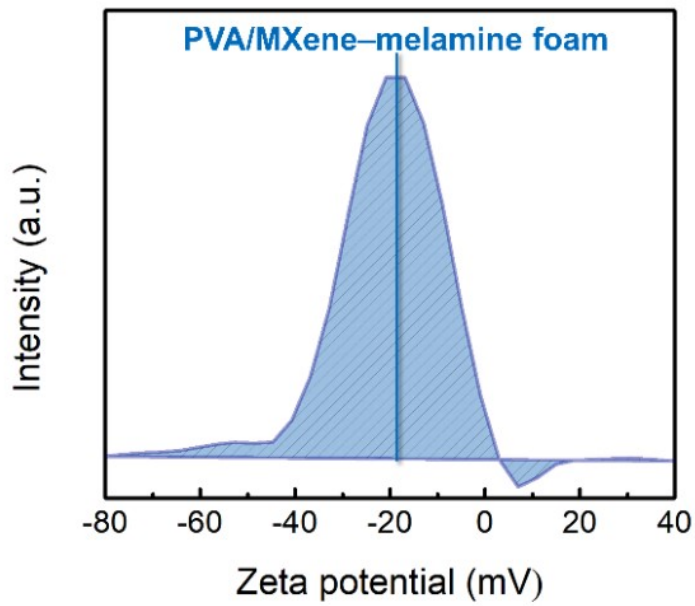
Fig. S17 Zeta potential distribution of the PVA/Mxene–melamine foam.
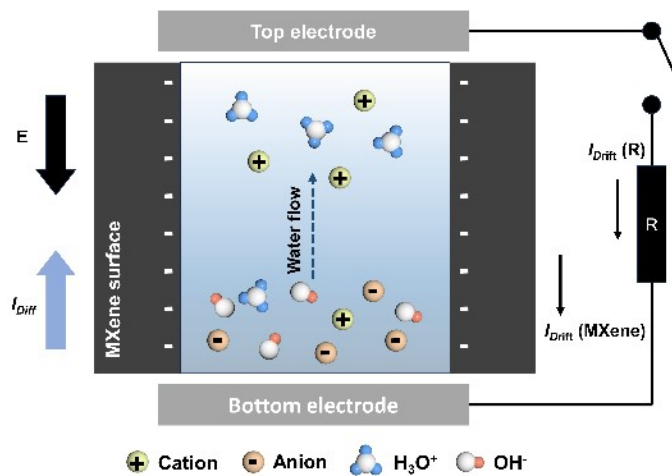
Fig. S18 Illustration of the mechanism for streaming potential and directional diffusion current influenced by flow dynamics.
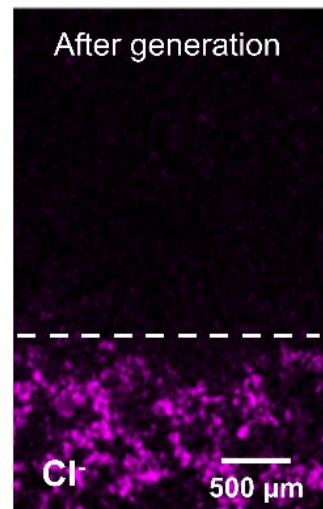
Fig. S19 Energy-dispersive X-ray spectroscopy (EDS) mapping of chloride ions on cross-section of MEG–MOHF after sustained power generation.
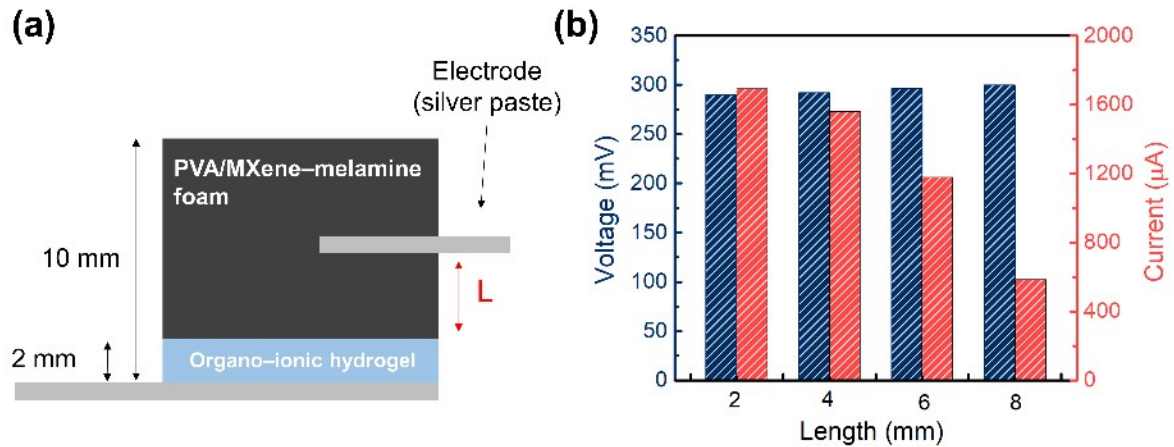
Fig. S20 Relationship between the length of the organo–ionic hydrogel and the inserted silver-coated polyethylene terephthalate (PET) electrode and the output performance of the MEG–MOHF. (a) Schematic illustration depicting the distance between the organo–ionic hydrogel and the inserted silver-coated PET electrode. (b) Corresponding open-circuit voltage (V_{OC}) and short-circuit current (I_{SC}), as a function of this length.
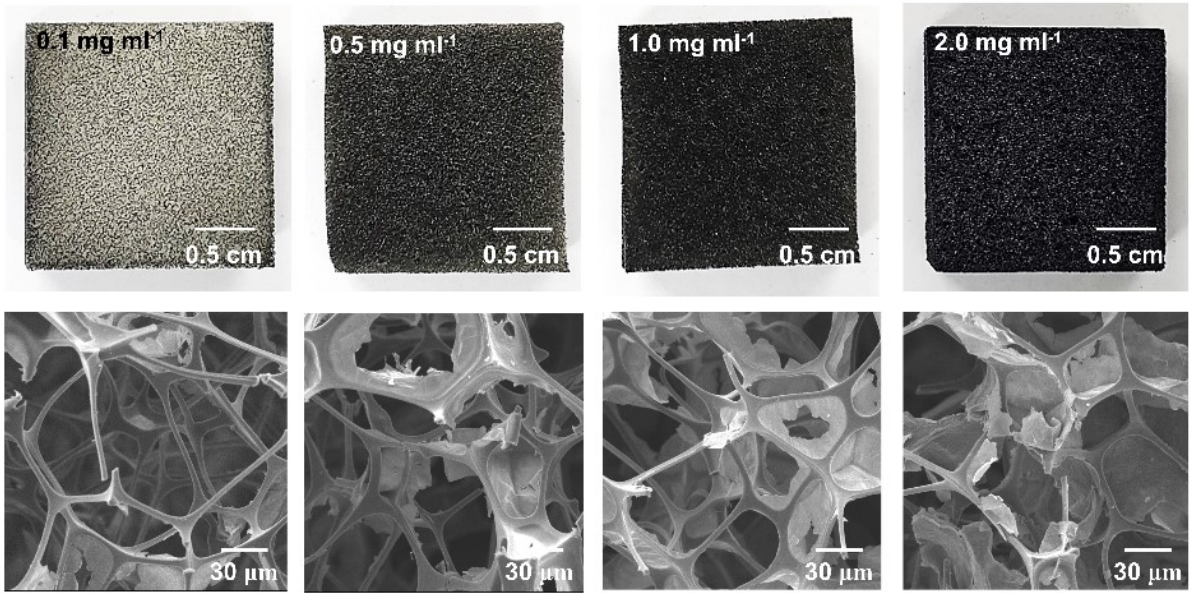
Fig. S21 Photographs and scanning electron microscopy (SEM) images of the melamine foam coated with different concentrations of Mxene.
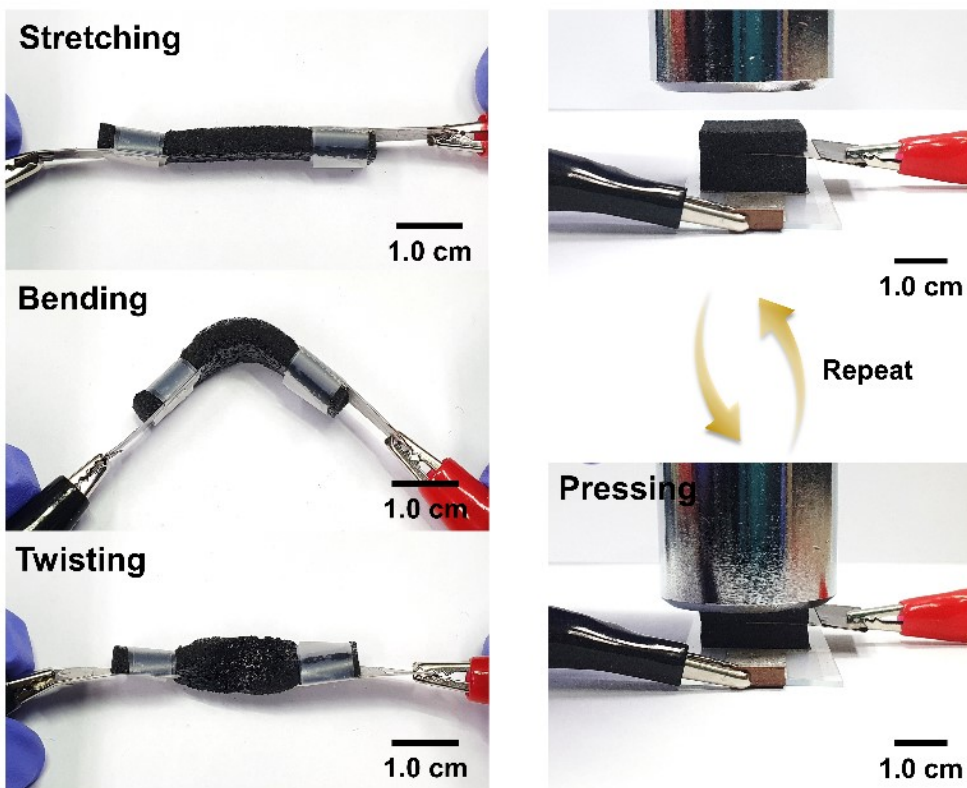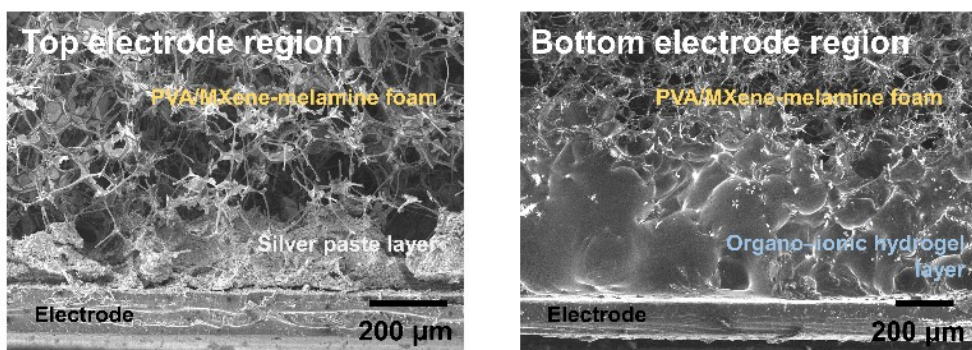
Fig. S22 (a) Evaluation of MEG–MOHF electrode stability under stretching, bending, twisting, and pressing. (b) SEM images of the electrode regions with MOHF after the deformations.
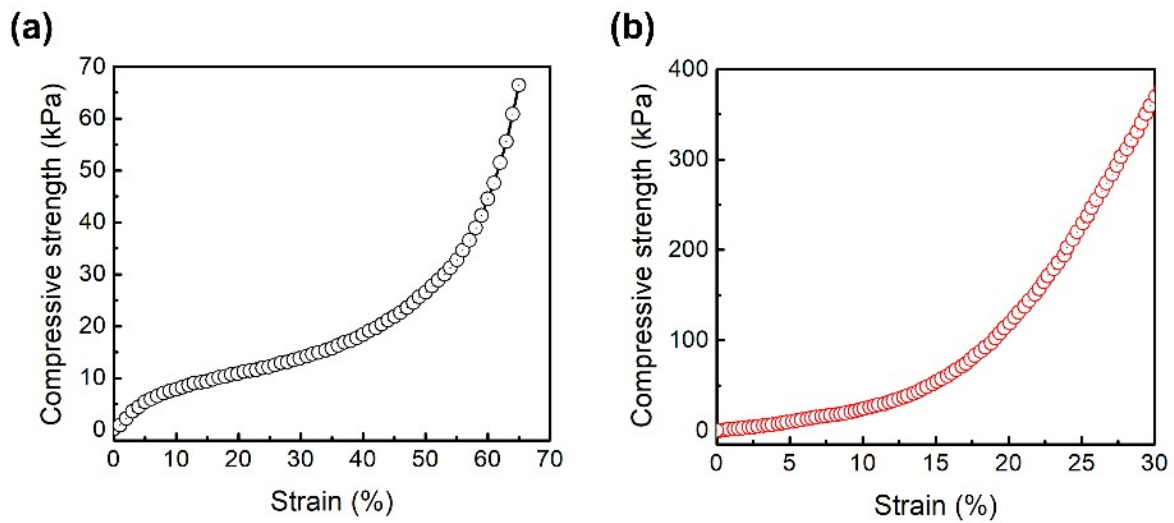
Fig. S23 Comparison of compressive strengths of (a) PVA/Mxene–melamine foam and (b) organo–ionic hydrogel-coated PVA/Mxene–melamine foam.
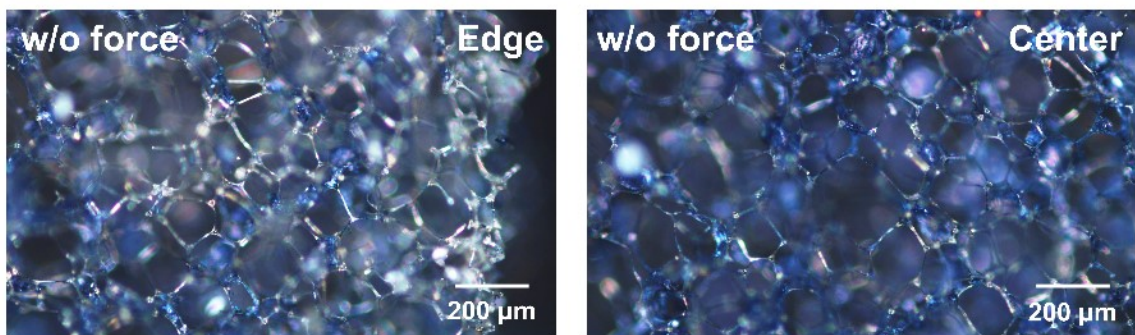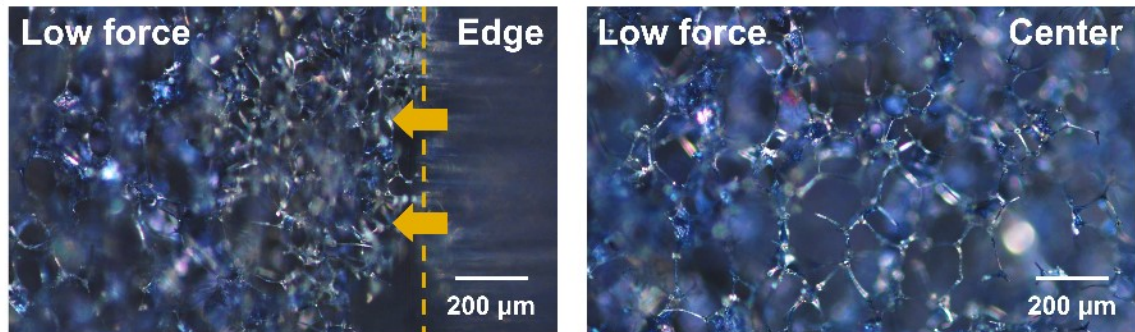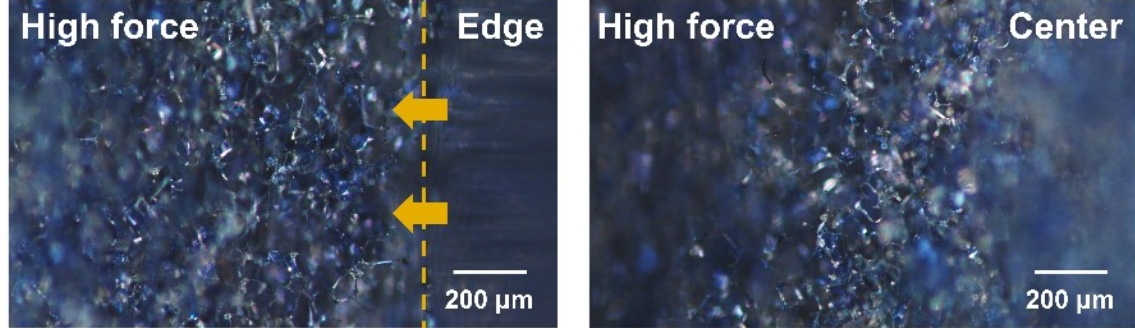
Fig. S24 Pore-size changes of top and center in MOHF (a) without force, (b) under low force (~15 kPa), and (c) under high force (~60 kPa).
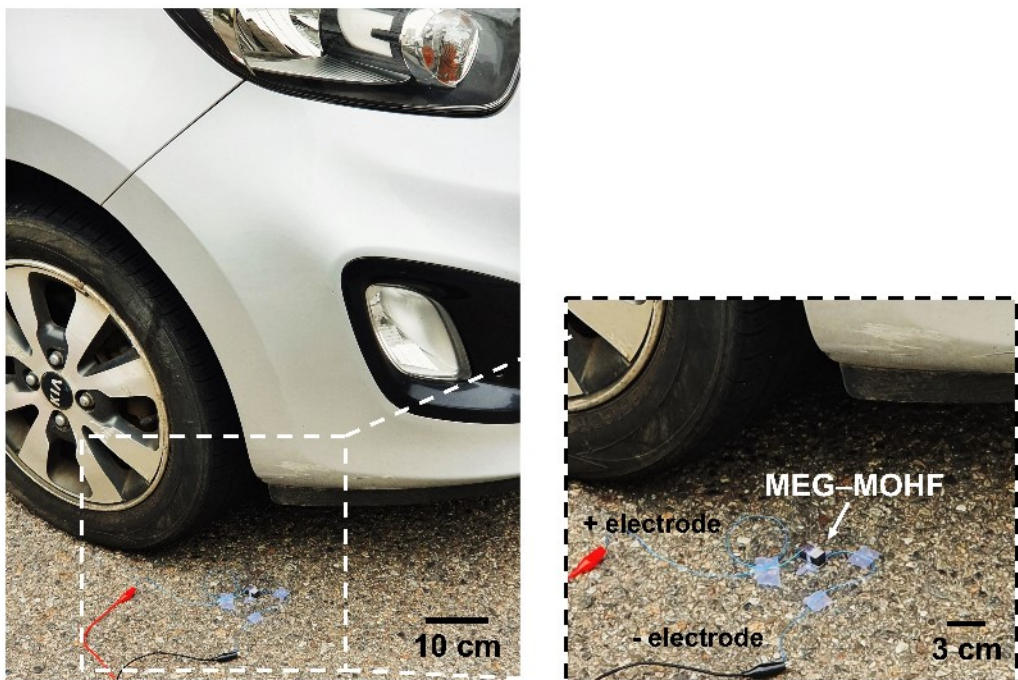
Fig. S25 Photographs of a MEG–MOHF under extreme pressure (~12.5 MPa) using commercial car.
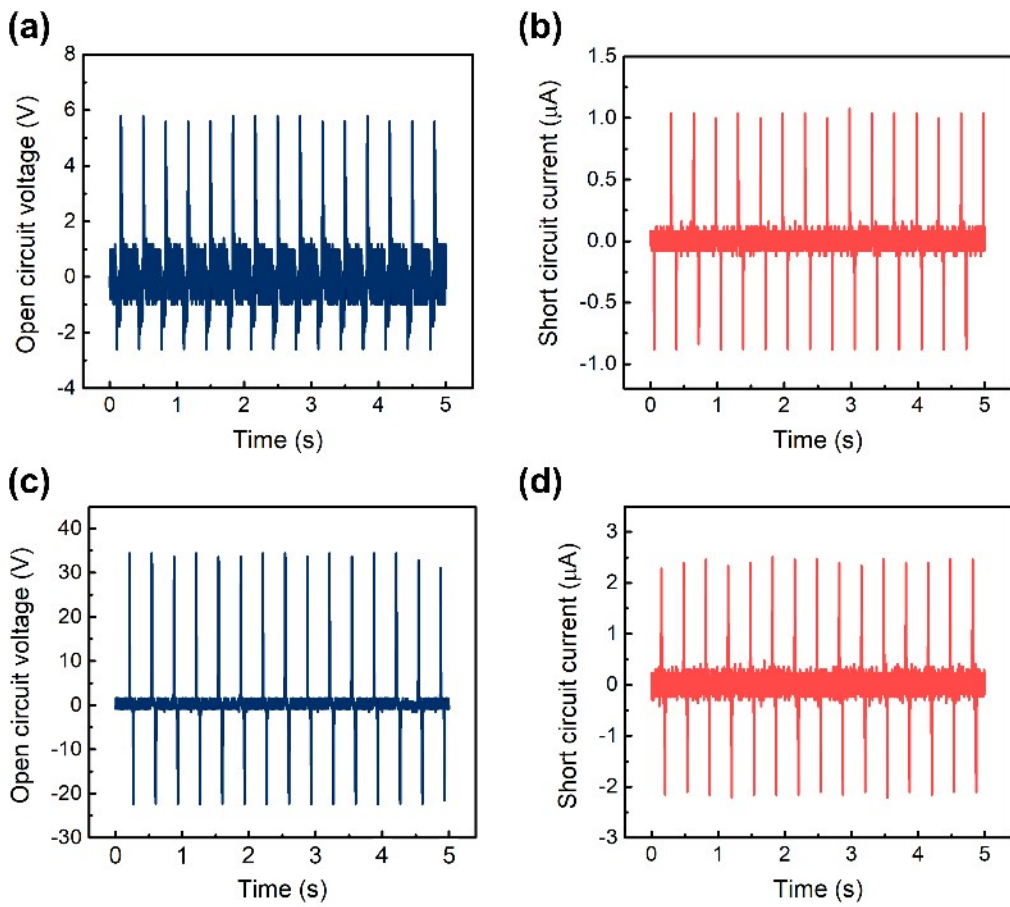
Fig. S26 Open-circuit voltage (V_{OC}) and short-circuit current (I_{SC}) of (a), (b) melamine foam and (c), (d) melamine foam coated with Mxene.
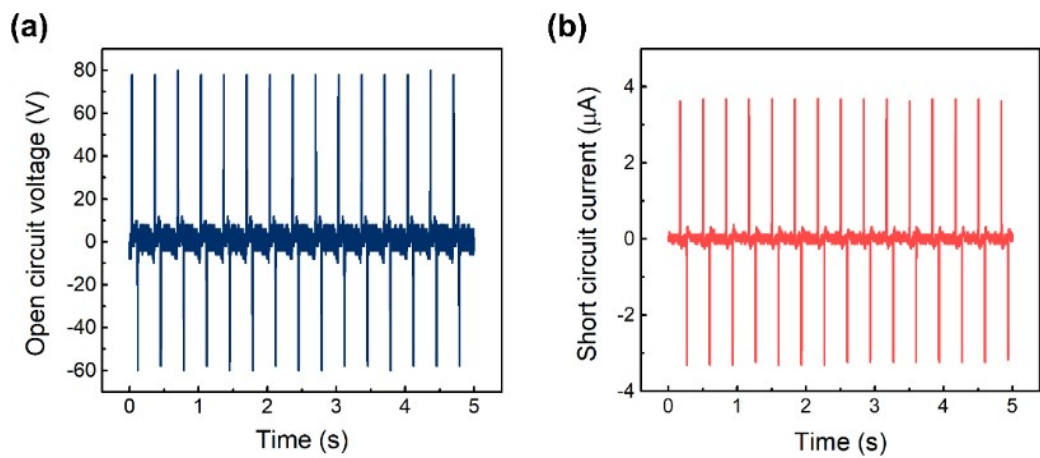
Fig. S27 (a) Open-circuit voltage (V_{OC}) and (b) short-circuit current (I_{SC}) of PVA/MXene–melamine foam.
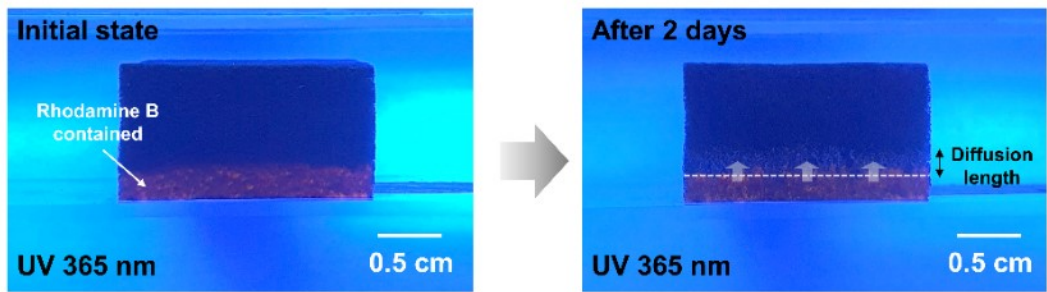
Fig. S28 Fluorescent photographs showing the diffusion of Rhodamine B containing water from an organo–ionic hydrogel in the MOHF.
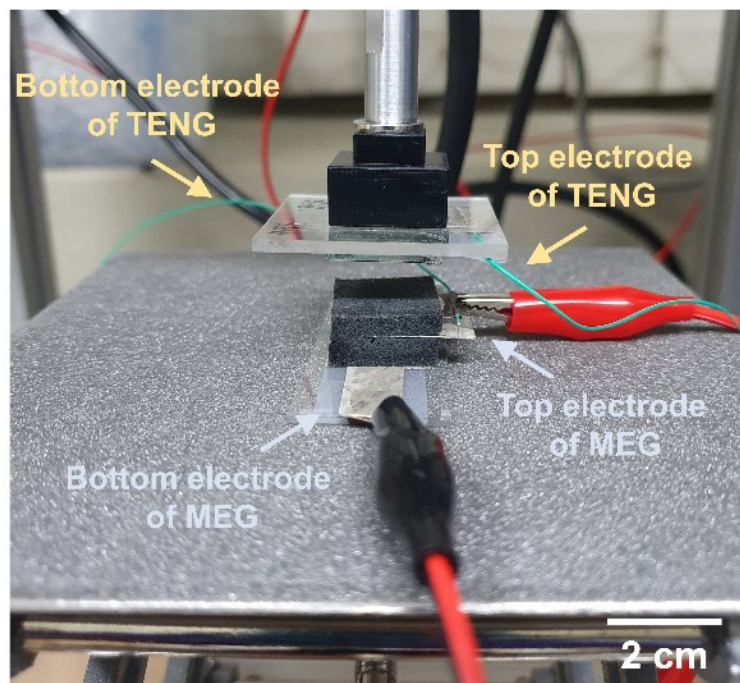
Fig. S29 Photograph of a complementary MEG–TENG–MOHF device.
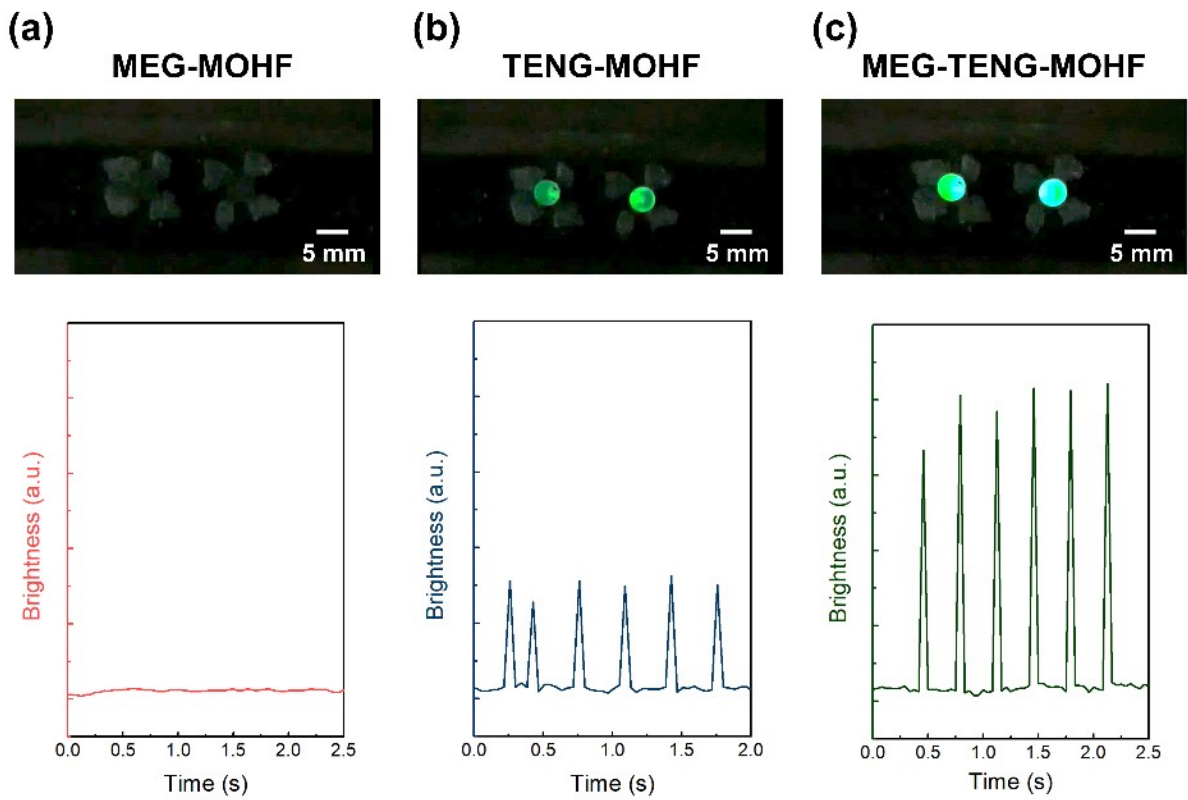
Fig. S30 Photographs and brightness signals of a photodetector from operating energy harvester of (a) MEG–MOHF, (b) TENG–MOHF, and (c) complementary MEG–TENG–MOHF single device.
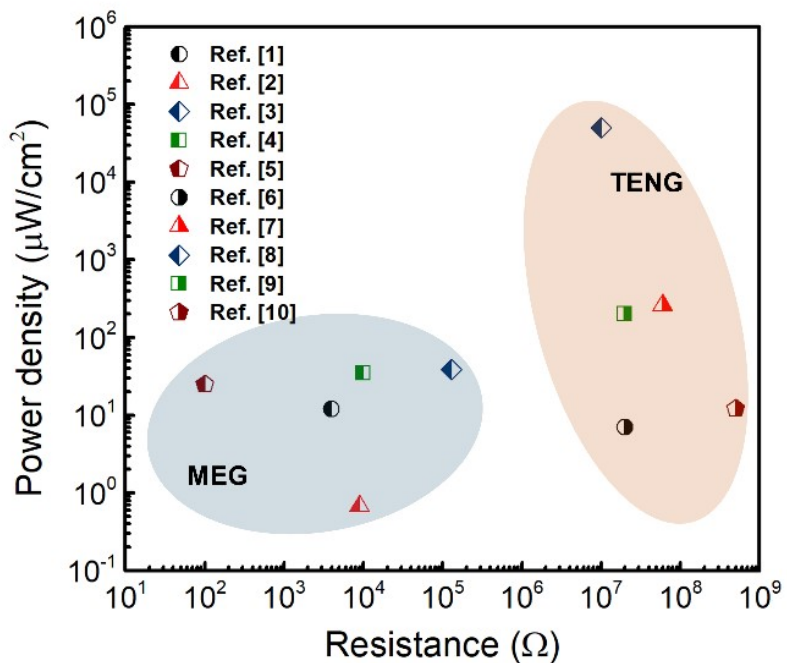
Fig. S31 Maximum power density values for the recent MEG and TENG works with optimal resistance values.

Reference

1 H. Wang, T. He, X. Hao, Y. Huang, H. Yao, F. Liu, H. Cheng and L. Qu, *Nat. Commun*, 2022, **13**, 2524.

2 L. Li, M. Hao, X. Yang, F. Sun, Y. Bai, H. Ding, S. Wang and T. Zhang, *Nano Energy*, 2020, **72**, 104663.

3 J. Liu, L. Huang, W. He, X. Cai, Y. Wang, L. Zhou and Y. Yuan, *Nano Energy*, 2022, **102**, 107709.

4 S. Yang, X. Tao, W. Chen, J. Mao, H. Luo, S. Lin, L. Zhang and J. Hao, *Adv. Mater.*, 2022, **34**, 2200693.

5 K. Zhao, J. W. Lee, Z. G. Yu, W. Jiang, J. W. Oh, G. Kim, H. Han, Y. Kim, K. Lee, S. Lee, H. Y. Kim, T. Kim, C. E. Lee, H. Lee, J. Jang, J. W. Park, Y. W. Zhang and C. Park, *ACS Nano*, 2023, **17**, 5472–5485.

6 Y. Liu, Y. Zheng, Z. Wu, L. Zhang, W. Sun, T. Li, D. Wang and F. Zhou, *Nano Energy*, 2021, **79**, 105422.

7 B. Yang, W. Zeng, Z. H. Peng, S. R. Liu, K. Chen and X. M. Tao, *Adv. Energy Mater.*, 2016, **6**, 1600505,

8 M. Kim, D. Park, M. M. Alam, S. Lee, P. Park and J. Nah, *ACS Nano*, 2019, **13**, 4640–4646.

9 H. Chen, Y. Xu, J. Zhang, W. Wu and G. Song, *Nanomaterials*, 2019, **9**, 778.

10 M. Cui, H. Guo, W. Zhai, C. Liu, C. Shen and K. Dai, *Adv. Funct. Mater.*, 2023, 2301589.
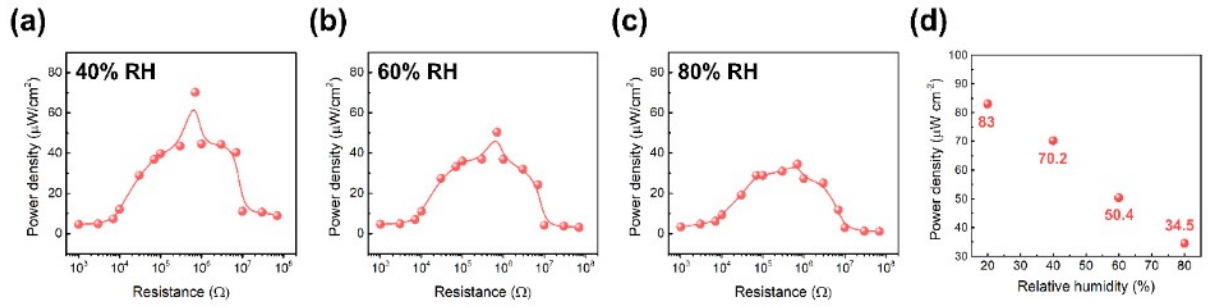
Fig. S32 Power density of MEG–TENG–MOHF depending on the load resistance at (a) 40% RH, (b) 60% RH and (c) 80% RH. (d) Dependence of the maximum power density of MEG–TENG–MOHF as a function of RH.
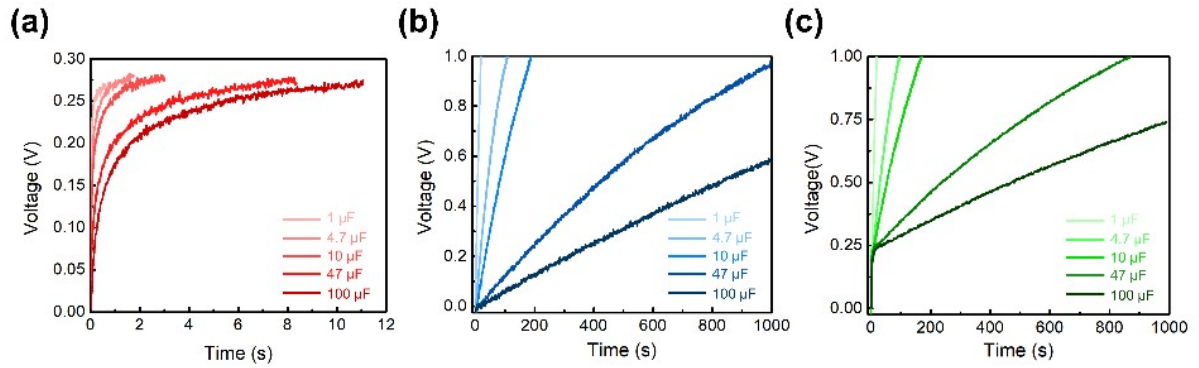
Fig. S33 Charging curves of capacitors with various capacities from (a) MEG–MOHF, (b) TENG–MOHF, and (c) complementary MEG–TENG–MOHF.
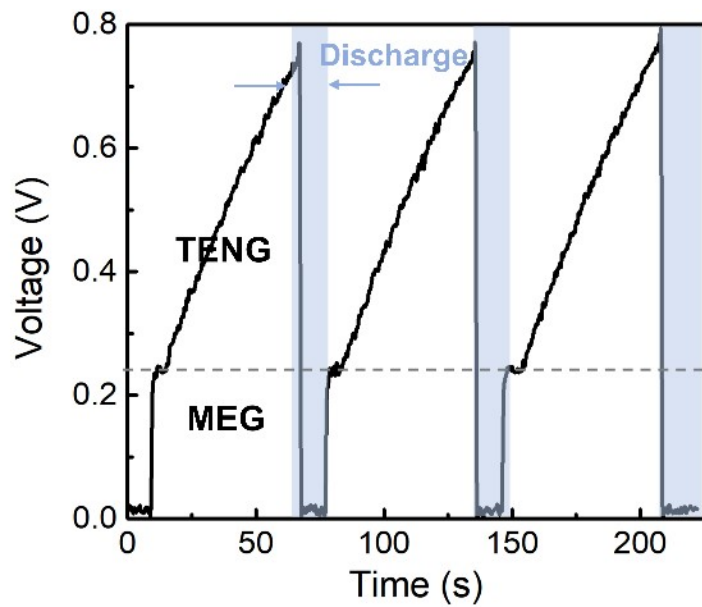
Fig. S34 Charging/discharging curves of commercial capacitor (4.7 µF) connected to a complementary MEG–TENG–MOHF.
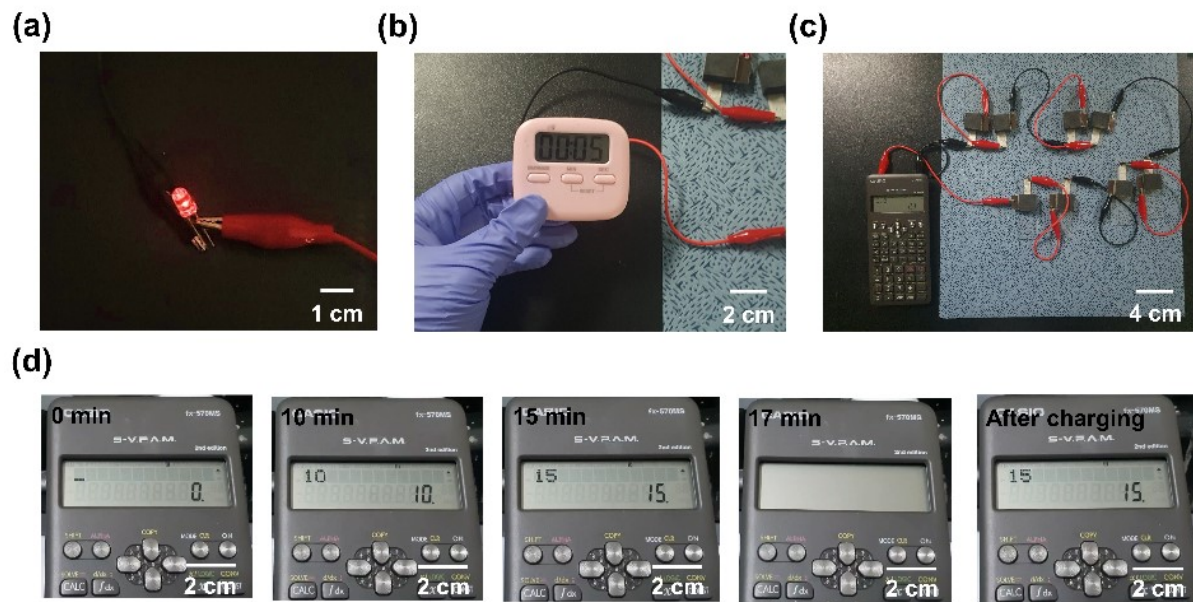
Fig. S35 Powering various commercial electronic devices by connecting eight-unit MEG–MOHFs in series: (a) an LED, (b) a watch, and (c) a calculator. (d) Long-term power supply capacity of the MEG–MOHF to operate the calculator.

Table S1. Characteristics of the recent electrical and mechanical properties of MEG and hybride MEG devices in comparison with the present work.

| Type	Material	Relative humidity (%)	Power Density (µW cm^{-2})	Stretching (strain%)	Compression (strain%, strenght)	Bending	Twisting	Reference
Film	CMC/MXene/Al^{3+}	90	-	O (8%)	O (8%, -)	O	X	1
	MXene/GO	100	-	O (0.4%)	O	X	X	2
	LiCl-loaded paper/CB	60	-	X	X	X	X	3
	Cellulose acetate nanofiber	90	2.45	O (35%)	X	X	X	4
	PSSA/PVA	85	7.9	O (25%)	X	O	O	5
	CNF/GO	85	-	O (4%)	X	O	O	6
	GO	70	27	X	X	O	O	7
	Defective ZIF-8/GO	37	109.2	X	X	X	X	8
Aerogel	GO/P-rGO aerogel	50	2.02	X	X	O	X	9
	IL-GO/GO@PVA aerogel	85	22.55	X	O (-, 80 kPa)	O	O	10
Fabric	PAN/PSSA nanofiber	80	1.48	X	X	O	O	11
	PVA ionic hydrogel-Carbon black fabric	70	70 µW cm^{-3}	O (~30%)	X	O	O	12
Hydrogel	LS-Al^{3+}-PAA hydrogel	55	0.24	O (>300%)	O (70%, 250 kPa)	O	O	13
	Nafion/pNIPAm hydrogel	80	10.14	X	X	X	X	14
	PVA-PA-glycerol hydrogel	85	35	X	X	O	X	15
Foam	PDMS/Carbon black/CNT	-	1	X	O (-, -)	X	X	16
	PVA@FCB@PU-sponge	55	2.7	X	X	O	X	17
Hybrid	PSSA/Kc (MEG-Sunlight)	70	~90	X	X	X	X	18
	PSSA/R (MEG-Sunlight)	50	88	O (~15%)	X	O	X	19
	PAMPS-PSSS (MEG-Thermoelectric generator)	60	4.75	O (~200%)	X	O	O	20
	Polyester-based yarn Cotton-based yarn (MEG-TENG)	-	MEG: 5.4 TENG: 166	O (25%)	X	O	X	21
	Silicon NW/Ag/FEP (MEG-TENG)	-	MEG: 8 TENG: 250	X	X	X	X	22
	MOHF (MEG-TENG)	20	MEG: 9.3 TENG: 28 MEG-TENG: 83	O (30%)	O (>95%, ~2.1 MPa)	O	O	This work

Reference

1 J. Wei, S. Jia, C. Ma, J. Guan, C. Yan, L. Zhao and Z. Shao, *Chem. Eng. J.*, 2023, **451**, 138565.

2 J. N. Ma, Y. L. Zhang, Y. Q. Liu, D. D. Han, J. W. Mao, J. R. Zhang, W. C. Zhao and H. B. Sun, *Sci. Bull.*, 2022, **67**, 501–511.

3 J. Tan, S. Fang, Z. Zhang, J. Yin, L. Li, X. Wang and W. Guo, *Nat. Commun.*, 2022, **13**, 3643.

4 J. Zhang, Y. Hou, L. Lei and S. Hu, *J. Memb. Sci.*, 2022, **662**, 120962.

5 H. Wang, H. Cheng, Y. Huang, C. Yang, D. Wang, C. Li and L. Qu, *Nano Energy*, 2020, **67**, 104238.

6 Z. Li, J. Wang, L. Dai, X. Sun, M. An, C. Duan, J. Li and Y. Ni, *ACS Appl. Mater. Interfaces*, 2020, **12**, 55205–55214.

7 Y. Liang, F. Zhao, Z. Cheng, Y. Deng, Y. Xiao, H. Cheng, P. Zhang, Y. Huang, H. Shao and L. Qu, *Energy Environ Sci.*, 2018, **11**, 1730–1735.

8 D. Lv, S. Zheng, C. Cao, K. Li, L. Ai, X. Li, Z. Yang, Z. Xu and X. Yao, *Energy Environ Sci.*, 2022, **15**, 2601–2609.

9 H. Cheng, Y. Huang, F. Zhao, C. Yang, P. Zhang, L. Jiang, G. Shi and L. Qu, *Energy Environ Sci.*, 2018, **11**, 2839–2845.

10 X. Zhang, M. Wang, Y. Wu, X. Chen, K. Wu, Q. Fu and H. Deng, *Adv. Funct. Mater.*, 2023, **33**, 2210027.

11 Z. Sun, L. Feng, X. Wen, L. Wang, X. Qin and J. Yu, *Mater. Horiz.*, 2021, **8**, 2303–2309.

12 Y. Zhang, S. Guo, Z. G. Yu, H. Qu, W. Sun, J. Yang, L. Suresh, X. Zhang, J. J. Koh and S. C. Tan, *Adv. Mater.*, 2022, **34**, 2201228.

13 J. Zhang, J. Zhuang, L. Lei and Y. Hou, *J. Mater. Chem. A*, 2023, **11**, 3546–3555.

14 C. Liu, S. Wang, X. Wang, J. Mao, Y. Chen, N. X. Fang and S. P. Feng, *Energy Environ Sci.*, 2022, **15**, 2489–2498.

15 S. Yang, X. Tao, W. Chen, J. Mao, H. Luo, S. Lin, L. Zhang and J. Hao, *Adv. Mater.*, 2022, **34**, 2200693.

16 J. H. Park, S. H. Park, J. Lee and S. J. Lee, *ACS Sustain. Chem. Eng.*, 2021, **9**, 5027–5037.

17 L. Li, M. Hao, X. Yang, F. Sun, Y. Bai, H. Ding, S. Wang and T. Zhang, *Nano Energy*, 2020, **72**, 104663.

18 J. Bai, Q. Liao, H. Yao, T. Guang, T. He, H. Cheng and L. Qu, *Energy Environ Sci.*, 2023, **16**, 3088-3097.

19 J. Bai, Y. Huang, H. Wang, T. Guang, Q. Liao, H. Cheng, S. Deng, Q. Li, Z. Shuai and L. Qu, *Adv. Mater.*, 2022, **34**, 2103897.

20 M. Yang, Y. Hu, S. Zheng, Z. Liu, W. Li and F. Yan, *Adv. Sci.*, 2023, **10**, 2206071.

21 J. Park, S. M. Chang, J. Shin, I. W. Oh, D. G. Lee, H. S. Kim, H. Kang, Y. S. Park, S. Hur, C. Y. Kang, J. M. Baik, J. S. Jang and H. C. Song, *Adv. Energy Mater.*, 2023, **13**, 2300530.

22 X. Chen, C. Jiang, Y. Song, B. Shao, Y. Wu, Z. Song, T. Song, Y. Wang and B. Sun, *Nano Energy*, 2022, **100**, 107495.